Chemical Research in Toxicology

Article

Cite This: Chem. Res. Toxicol. XXXX, XXX, XXX−XXX

pubs.acs.org/crt

Structure−Activity Relationships for CYP4B1 Bioactivation of 4-Ipomeanol Congeners: Direct Correlation between Cytotoxicity and Trapped Reactive Intermediates

John P. Kowalski,[†] Matthew G. McDonald,[†] Dale Whittington,[†] Miklos Guttman,[†] Michele Scian,[†] Marco Girhard,[‡] Helmut Hanenberg,[§] Constanze Wiek,[⊥] and Allan E. Rettie*[,†]

[†]Department of Medicinal Chemistry, School of Pharmacy, University of Washington, Seattle, Washington 98105, United States

[‡]Institute of Biochemistry, Heinrich-Heine University, 40225 Düsseldorf, Germany

[§]Department of Pediatrics III, University Children's Hospital Essen, University of Duisburg-Essen, 45122 Essen, Germany

[⊥]Department of Otorhinolaryngology and Head/Neck Surgery, Heinrich-Heine University, 40225 Düsseldorf, Germany

Supporting Information

ABSTRACT: Cytochrome P450 4B1 (CYP4B1) has been explored as a candidate enzyme in suicide gene systems for its ability to bioactivate the natural product 4-ipomeanol (IPO) to a reactive species that causes cytotoxicity. However, metabolic limitations of IPO necessitate discovery of new "pro-toxicant" substrates for CYP4B1. In the present study, we examined a series of synthetically facile *N*-alkyl-3-furancarboxamides for cytotoxicity in HepG2 cells expressing CYP4B1. This compound series maintains the furan warhead of IPO while replacing its alcohol group with alkyl chains of varying length (C1−C8). Compounds with C3−C6 carbon chain lengths showed similar potency to IPO ($LD_{50} \approx 5\ \mu M$). Short chain analogs (<3 carbons) and long chain analogs (>6 carbons) exhibited reduced toxicity, resulting in a parabolic relationship between alkyl chain length and cytotoxicity. A similar parabolic relationship was observed between alkyl chain length and reactive intermediate formation upon trapping of the putative enedial as a stable pyrrole adduct in incubations with purified recombinant rabbit CYP4B1 and common physiological nucleophiles. These parabolic relationships reflect the lower affinity of shorter chain compounds for CYP4B1 and increased ω-hydroxylation of the longer chain compounds by the enzyme. Furthermore, modest time-dependent inhibition of CYP4B1 by *N*-pentyl-3-furancarboxamide was completely abolished when trapping agents were added, demonstrating escape of reactive intermediates from the enzyme after bioactivation. An insulated CYP4B1 active site may explain the rarely observed direct correlation between adduct formation and cell toxicity reported here.

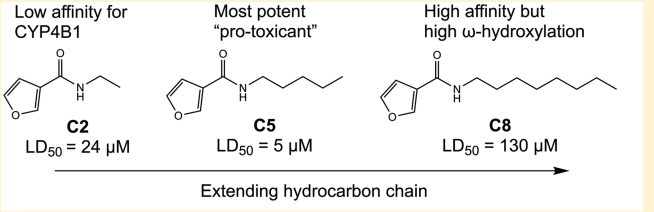

INTRODUCTION

The cytochrome P450 4 (CYP4) family consists of 13 enzymes in humans that are typically involved in fatty acid and eicosanoid oxidation.[1] CYP4B1 is considered an orphan isozyme in the family, with unknown endogenous substrate selectivity.[2] In humans, CYP4B1 is catalytically deficient due to low stability caused, in part, by a Pro-to-Ser change in the meander region of the enzyme.[3,4] However, other mammalian orthologs, present in cattle and rabbit, exhibit good stability and bioactivate several protoxins that induce toxicological effects in expression-specific tissues.[2]

4-Ipomeanol (IPO), produced by the common sweet potato in response to stress, is a 3′-substituted furan-containing natural product, which is bioactivated by pulmonary CYP4B1 to an electrophilic species that binds tissue nucleophiles to elicit its organ toxicity.[5] Consequently, IPO and related furans, like perilla ketone (PK), have been suggested as cytotoxic prodrugs in a novel CYP4B1 suicide gene system in humans. Introduction of exogenous and functional (e.g., rabbit) CYP4B1 could theoretically allow for controlled cytotoxicity relegated to where this bioactivating enzyme is newly expressed. Specifically, this may have utility in an anticancer setting as a molecular switch for T-cell inactivation[6] since adverse immunological responses pose serious safety issues that can limit T-cell therapy.[7−9] Use of mammalian CYP4B1 as a suicide gene could potentially reduce the immunogenicity that arises from other systems like the herpes simplex virus thymidine kinase and ganciclovir tandem.[6]

However, IPO and PK possess structural features that could negatively impact their metabolism, thereby limiting their duration of action or effectiveness. Rodent studies suggest rapid clearance of IPO by glucuronidation,[10,11] and several human uridine 5′-diphosphoglucuronosyl transferases (UGTs) are known to conjugate IPO.[12] While PK lacks this alcohol moiety, replacement by a methyl group confers extensive CYP4B1-mediated oxidation to nonreactive products.[13] This latter observation suggests that CYP4B1 can bind alkyl furans

Received: August 9, 2019

DOI: 10.1021/acs.chemrestox.9b00330
Chem. Res. Toxicol. XXXX, XXX, XXX−XXX

in distinct catalytic orientations that influence the bioactivation versus inactivation processes.

The goal of this study is to clarify the relationship between 3′-substituted furan structure and CYP4B1-mediated metabolism to either reactive intermediates (derived from oxidation of the furan group) or nonreactive metabolites (derived from oxidation of the alkyl group). In preliminary studies, we probed the CYP4B1 permissible chemical space for furan-containing substrates using a high-throughput cytotoxicity screen performed with CYP4B1-transfected HepG2 cells and a mini-library of >400 IPO-like compounds (data not shown). Although no compounds proved as potent as IPO, *N*-alkyl-3-furancarboxamides emerged as a common motif in the hits from this library. Therefore, we adopted a simple synthetic approach to generate a homologous series of eight *N*-alkyl-3-furancarboxamides and evaluated their CYP4B1-mediated cytotoxicity. Structure−metabolism relationships are discussed, and the lack of mechanism-based inhibition of CYP4B1 by 3′-substituted furans was identified as a key determinant of the efficiency of the cytotoxic process.

EXPERIMENTAL PROCEDURES

General Reagents. Recombinant rabbit CYP4B1 was expressed in *Escherichia coli* and purified using an established protocol.[14] Cytochrome P450 reductase (CPR) and cytochrome b5 coenzymes used in CYP4B1 incubations were expressed and purified according to previously published methods.[15] Chloroform-d ($CDCl_3$) and deuterium oxide (D_2O) used for NMR experiments were purchased from Cambridge Isotope Laboratories, Inc. (Andover, MA). Reduced β-nicotinamide-adenine dinucleotide phosphate (NADPH) for CYP4B1 incubations was purchased from OYC Americas (Vista, CA). 1,2-Dilauroyl-*sn*-glycero-3-phosphocholine (DLPC) for CYP4B1 incubations was purchased from Avanti Polar Lipids (Alabaster, AL). Tissue culture supplies (Gibco) and organic solvents were purchased from Thermo-Fisher Scientific (Pittsburgh, PA), and all other chemicals were obtained from Sigma-Aldrich (St. Louis, MO).

Whole Cell Measurement of CYP4B1-Mediated Toxicity. A cell proliferation assay was used to assess the cytotoxicity of compounds **C1**−**C8**. HepG2 cells were modified by lentiviral transduction to express rabbit CYP4B1, or a control vector, as previously described.[4,6,11,16] Western blot analysis of the cell lines showed ∼130 pmol CYP4B1/mg of lysate protein and no detectable enzyme in the control vector line. Enzyme levels were quantitated using recombinantly expressed purified rabbit CYP4B1 as a standard (Figure S1). Stably transduced cells were grown in tissue culture media (DMEM, 10% FBS, 1% pen/strep, and 10 mM HEPES) and selected with puromycin treatment (2 μg/mL) over a 7-day period. Cells were seeded into white-walled 96-well plates at 10 000 cells/well and grown for 24 h. Both cell lines were then treated with **C1**−**C8** at eight doses spanning the following concentrations: **C1** 0.55−1200 μM, **C2** 0.14−300 μM. **C3**−**C6** 0.4−50 μM, **C7** 0.14−300 μM, **C8** 1.6−150 μM (DMSO did not exceed 0.1%). Cells were incubated for 72 h, and the viability was determined with the CellTiter-Glo Luminescent Assay (Promega, Madison, WI). Vehicle-treated wells were set to 100% viability, and lethal dose 50% (LD_{50}) values were calculated from dose−response curves using nonlinear regression curve fitting with GraphPad Prism 7.00.

Chemical Synthesis. The general method for *N*-alkyl-3-furancarboxamides was performed as follows. A solution containing 1 equiv (eq) of 3-furoic acid, 2 eq of thionyl chloride, and a catalytic amount of DMF in anhydrous dichloromethane (DCM) was refluxed for 3 h to generate a crude batch of 3-furoyl chloride. Solvent and excess thionyl chloride were evaporated, and the 3-furoyl chloride was used in the following step without further workup. A solution of 3-furoyl chloride in DCM was next cooled over ice, and 2 eq of the aliphatic amine (ethyl-, through octyl-amine), along with a catalytic amount of pyridine, was added dropwise. Reactions were stirred overnight at room temperature, quenched with water, extracted with ethyl acetate, and dried over magnesium sulfate. Compounds were isolated via flash chromatography using a hexane/ethyl acetate gradient. Purity assessed by LC−MS/UV and ^{1}H NMR were >95% for all compounds. ^{1}H NMR experiments were performed at 25 °C on a 499.73 MHz Agilent DD2 spectrometer. For characterization and spectral assignment purposes, the samples were ∼30 mM solutions in $CDCl_3$ (99.96% D, Cambridge Isotopes). Chemical shifts are reported below relative to the solvent peak in $CDCl_3$ at 7.26 ppm, and the coupling constants (J) are noted in hertz (Hz). All annotated ^{1}H NMR spectra have been provided in the Supporting Information. Accurate mass analyses of the compounds were determined via LC−MS on a Thermo LTQ-Orbitrap mass spectrometer.

N-Ethyl-3-furancarboxamide, ***C2***. Exact mass [M + H] calculated 140.0712, observed 140.0698, δ ppm 9.7. ^{1}H NMR ($CDCl_3$), 7.91 (s, 1H), 7.42 (s, 1H), 6.59 (s, 1H), 5.75 (bs, 1H), 3.46−3.42 (m, 2H), 1.22 (t, J = 7.5 Hz, 3H). Yield 58%.

N-Propyl-3-furancarboxamide, ***C3***. Exact mass [M + H] calculated 154.0868, observed 154.0871, δ ppm 1.9. ^{1}H NMR ($CDCl_3$), 7.94 (s, 1H), 7.39 (s, 1H), 6.67 (s, 1H), 6.51 (bs, 1H), 3.31 (q, J = 7 Hz, 2H), 1.56 (sx, J = 7.5 Hz, 2H), 0.92 (t, J = 7 Hz, 3H). Yield 56%.

N-Butyl-3-furancarboxamide, ***C4***. Exact mass [M + H] calculated 168.1025, observed 168.1022, δ ppm 1.5. ^{1}H NMR ($CDCl_3$), 7.95 (s, 1H), 7.36 (s, 1H), 6.88 (bs, 1H), 6.70 (s, 1H), 3.31 (q, J = 7 Hz, 2H), 1.50 (p, J = 7.5 Hz, 2H), 1.31 (sx, J = 7.5 Hz, 2H), 0.86 (t, J = 7.5 Hz, 3H). Yield 65%.

N-Pentyl-3-furancarboxamide, ***C5***. Exact mass [M + H] calculated 182.1181, observed 182.1170, δ ppm 6.1. ^{1}H NMR ($CDCl_3$), 7.94 (s, 1H), 7.46 (s, 1H), 6.62 (s, 1H), 5.76 (bs, 1H), 3.43 (q, J = 7 Hz, 2H), 1.62 (p, J = 7.5 Hz, 2H), 1.39 (m, 4H), 0.94 (t, J = 7 Hz, 3H). Yield 70%.

N-Hexyl-3-furancarboxamide, ***C6***. Exact mass [M + H] calculated 196.1338, observed 196.1333, δ ppm 2.3. ^{1}H NMR ($CDCl_3$), 7.94 (s, 1H), 7.39 (s, 1H), 6.66 (s, 1H), 6.41 (bs, 1H), 3.35 (t, J = 7 Hz, 2H), 1.54 (p, J = 7.5 Hz, 2H), 1.29 (m, 6H), 0.86 (t, J = 7 Hz, 3H). Yield 64%.

N-Heptyl-3-furancarboxamide, ***C7***. Exact mass [M + H] calculated 210.1494, observed 210.1484, δ ppm 4.8. ^{1}H NMR ($CDCl_3$), 7.94 (s, 1H), 7.46 (s, 1H), 6.62 (s, 1H), 5.76 (bs, 1H), 3.43 (q, J = 7 Hz, 2H), 1.61 (p, J = 7 Hz, 2H), 1.34 (m, 8H), 0.91 (t, J = 7 Hz, 3H). Yield 69%.

N-Octyl-3-furancarboxamide, ***C8***. Exact mass [M + H] calculated 224.1651, observed 224.1643, δ ppm 3.4. ^{1}H NMR ($CDCl_3$),7.94 (s, 1H), 7.38 (s, 1H), 6.67 (s, 1H), 6.52 (bs, 1H), 3.34 (q, J = 7 Hz, 2H), 1.54 (p, J = 7.5 Hz, 2H), 1.27 (m, 10H), 0.85 (t, J = 7 Hz, 3H). Yield 48%.

N-(2-Hydroxyethyl)-3-furancarboxamide, ***C2-OH***. Exact mass [M + H] calculated 156.0655, observed 156.0652, δ ppm 1.9. ^{1}H NMR ($CDCl_3$), 7.95 (s, 1H), 7.43 (s, 1H), 6.63 (s, 1H), 6.33 (bs, 1H), 3.82 (s, 2H), 3.59 (s, 2H). Yield 42%.

N-(2-Hydroxypentyl)-3-furancarboxamide, ***C5-OH***. Exact mass [M + H] calculated 198.1125, observed 198.1126, δ ppm 0.6. ^{1}H NMR ($CDCl_3$), 7.93 (s, 1H), 7.43 (s, 1H), 6.61 (s, 1H), 5.94 (bs, 1H), 3.67 (t, J = 6.5 Hz, 2H), 3.43 (q, J = 7 Hz, 2H), 1.74 (bs, 1H), 1.64 (sx, J = 7 Hz, 4H), 1.47 (m, 2H). Yield 46%.

N-(2-Hydroxyoctyl)-3-furancarboxamide, ***C8-OH***. Exact mass [M + H] calculated 240.1594, observed 240.1595, δ ppm 0.4. ^{1}H NMR ($CDCl_3$), 7.92 (s, 1H), 7.43 (s, 1H), 6.61 (s, 1H), 5.84 (bs, 1H), 3.64 (t, J = 6.5 Hz, 2H), 3.4 (q, J = 7 Hz, 2H), 1.67 (bs, 1H), 1.58 (sx, J = 7.5 Hz, 4H), 1.35 (m, 8H). Yield 35%.

N-Methyl-3-furancarboxamide, ***C1***. Synthesis of C1 was performed as previously described.[17] Briefly, 1 eq of 3-furoic acid, 1.2 eq of EDC-HCl, 0.3 eq of HOBt, and 1.05 eq of $MeNH_3Cl$ were placed in a sealed flask flushed with nitrogen. MeCN was added, and the solution was stirred for 5 min, followed by addition of 1.05 eq of Et_3N. The reaction was stirred for 1.5 h, and water was added prior to workup. The mixture was extracted thrice with ethyl acetate followed by a brine wash, then dried over magnesium sulfate and purified via

DOI: 10.1021/acs.chemrestox.9b00330
Chem. Res. Toxicol. XXXX, XXX, XXX−XXX

flash chromatography with a hexane/ethyl acetate gradient. Exact mass [M + H] calculated 126.0550, observed 126.0553, δ ppm 2.4. ^{1}H NMR, 7.92 (s, 1H), 7.43 (s, 1H), 6.60 (s, 1H), 2.96 (s, 3H). Yield 65%.

*Glutathione (GSH)/N-α-Acetyl-L-lysine (NAL) **C5** Adduct Standard, **C5-GSH/NAL**.* A modified synthesis procedure that has been published was utilized.[18] To a mixture of 1 eq of compound **C5** in a 1:1 solution of saturated aqueous $NaHCO_3$/acetone was added 1.1 eq of potassium peroxymonosulfate. The *in situ* generation of dimethyldioxirane and oxidation of **C5** was allowed to proceed for 30 min at room temperature with stirring. Subsequently, 1.1 eq of GSH and 2 eq of NAL were added, and the reaction allowed to proceed for 1 h at 70 °C. Upon cooling, the precipitates were filtered out, and the crude mixture was subjected to semipreparative HPLC purification on a Phenomenex (Torrance, CA) Luna C18 column (10 × 250 mm^2, 5 μm, 100 Å), starting with 95% mobile phase A (0.1% formic acid in H_2O) and 5% mobile phase B (0.1% formic acid in acetonitrile) at a flow rate of 5 mL/min. After holding for 5 min, B was increased linearly from 5 to 30% between 5 and 30 min, then B was increased linearly from 30 to 50% between 30 and 35 min. At 35.01 min, B was increased to 95% and held for 5 min; total run time was 45 min following a 5 min equilibration period. The synthetic standard was characterized by high resolution LC−MS/MS and 2D-NMR techniques (Figure S3 and S4). Exact mass [M + H] calculated 657.2912, observed 657.290 (δ ppm 1.3). Yield 16%.

GSH/NAL Trapping and Adduct Comparison of CYP4B1-Generated Reactive Intermediates from Compounds C1−C8. Metabolic incubations contained 25 pmol purified rabbit CYP4B1, 50 pmol CPR, 25 pmol cytochrome b5, 2.5 μg of DLPC, 100 U catalase, 50 μg of superoxide dismutase, 5 mM NAL, and 5 mM GSH in 50 mM potassium phosphate buffer (KPi), pH 7.4, in a final volume of 100 μL, similar to as reported previously.[13] Compounds **C1−C8** were added to achieve a final concentration of 100 μM. After 30 min reconstitution on ice, metabolic reactions were initiated by the addition of NADPH (1 mM final concentration) and allowed to progress for 30 min at 37 °C. Reactions were quenched with an equal volume of acetonitrile containing 2 μM furafylline as the internal standard and centrifuged at 16 000*g* for 5 min. A supernatant aliquot (10 μL) was analyzed by UPLC−MS/MS on a Waters Acquity UPLC (Milford, MA) connected to a Xevo TQ-S instrument in ESI+ mode, with the following settings: capillary 3.50 kV, cone 30.0 V, collision 10.0 V, source offset 60.0 V, source temperature 150 °C, desolvation temperature 350 °C, cone gas flow 150 L/h, desolvation gas flow 800 L/hour, and collision gas flow 0.15 mL/min. Analytes were separated chromatographically using a Waters HSS T3 column (2.1 × 100 mm^2, 1.8 μm), starting with 95% mobile phase A (0.1% formic acid in H_2O) and 5% mobile phase B (0.1% formic acid in acetonitrile) at a flow rate of 0.3 mL/min. After holding for 1 min, B was increased linearly from 5 to 95% between 1 and 7 min and held at 95% between 7 and 10 min; total run time was 12 min following a 2 min equilibration period. Under these conditions, the eight different GSH/NAL adducts eluted at 3.2, 3.4, 3.6, 3.8, 4.0, 4.2, 4.5, and 4.7 min for **C1−C8**, respectively, and were detected with neutral loss scanning of 129 Da (NL129). Windows spanning 5 Da were set for each compound, surrounding the parent m/z for each adduct. The internal standard, furafylline, was eluted at 4.1 min and was detected by multiple reaction monitoring (MRM) at m/z 261.3 > 81.0. Peak area ratios (PAR) for each adduct were determined by dividing the peak areas of the analytes by that of furafylline, and metabolite analysis was performed with MassLynx V4.1.

Kinetics of Metabolite Formation by CYP4B1. Metabolic incubations contained the same reconstituted enzyme mixture as outlined above in the above. Concentrations of **C2**, **C5**, and **C8** spanned 50−3000, 1−300, and 1−100 μM, respectively. The reactions were initiated by the addition of NADPH (1 mM final concentration) and allowed to progress for 15 min at 37 °C, followed by the same workup described above in the GSH/NAL trapping experiments. Chromatographic separation of **C5-OH**, **C5-Adduct**, and **C8-OH** utilized the same instrument, column, and LC method as described above. A Xevo TQ-S instrument was set to ESI+ mode with the following settings: capillary 3.50 kV, cone 30.0 V, collision 10.0 V, source offset 60.0 V, source temperature 150 °C, desolvation temperature 350 °C, cone gas flow 150 L/h, desolvation gas flow 800 L/h, and collision gas flow 0.15 mL/min. Using these conditions, **C5-OH**, **C5-Adduct**, and **C8-OH** eluted at 3.7, 4.1, and 4.7 min and were detected, respectively, in the following channels by MRM: m/z 198.1 > 95.1, 657.2 > 528.1, and 240.2 > 95.1. **C5-Adduct** was also detected via NL129 with results practically identical to that obtained with MRM. Separation of **C2-OH** was also achieved with a gradient of 0.1% formic acid in H_2O (solvent A) and 0.1% formic acid in acetonitrile (solvent B) at a flow rate of 0.3 mL/min. After holding at 2% for 3 min, B was increased linearly to 95% between 3 and 9 min and held at 95% between 9 and 10 min. The total run time was 12 min following a 2 min equilibration period. **C2-OH** eluted at 4.9 min and was detected by MRM at m/z 156.1 > 95.1. Calibration standards for **C2-OH**, **C5-OH**, **C5-Adduct**, and **C8-OH** were prepared in blank incubation matrix from DMSO stocks and metabolite analysis was performed with MassLynx V4.1.

Characterization of C5-Adduct Isomers. Metabolic incubations contained 50 pmol purified rabbit CYP4B1, 100 pmol CPR, 50 pmol cytochrome b5, 5 μg of DLPC, 100 U catalase, 50 μg of superoxide dismutase, 5 mM NAL, and 5 mM GSH in 50 mM KPi, pH 7.4, in a final volume of 100 μL. Compound **C5** was added to achieve a final concentration of 200 μM, and then the same incubation and workup procedure described above in the GSH/NAL trapping experiments was used. A supernatant aliquot (10 μL) was analyzed by UPLC−MS/MS on a Waters Acquity UPLC connected to an AB Sciex Triple TOF 5600 (Framingham, MA) set to ESI+ mode with the following settings. Ion source gas 1, 60 arbitrary units (au); ion source gas 2, 60 au; curtain gas, 35 au; temperature, 600 °C; ionspray voltage, 4500 V; declustering potential, 100 V; collision energy, 35 V; collision energy spread, 20 V; ion release delay, 67 au; and ion release width, 25 au. Isomers were separated chromatographically using a Tosoh Biosciences (Tokyo, Japan) TSKgel ODS-100 V column (2.0 × 150 mm^2, 3 μm), starting with 100% mobile phase A (0.2% acetic acid in H_2O) at a flow rate of 0.2 mL/min. After a 2 min hold, mobile phase B (0.2% acetic acid in methanol) was increased linearly from 0 to 60% between 2 and 50 min, then ramped to 100% B rapidly and held at 100% B from 50.1 to 56 min. Total run time was 60 min following a 4 min equilibration period. Using these conditions, isomers numbered 1, 2, 3, and 4 eluted at retention times (RT) of 40.0, 40.8, 41.9, and 42.4 min, respectively. Analytes were detected by both TOF MS positive mode using a 50−1000 Da window and positive mode product ion scanning from the parent ion of m/z 657.29 Da.

CYP4B1 Substrate Docking. Substrate docking was performed in AutoDock Vina[19] using the crystal structure of rabbit CYP4B1[20] (PDB 5T6Q). Models of **C2**, **C5**, and **C8** were generated in Open Babel[21] at pH 7.4, and the substrate and protein files were processed using AutoDock tools. Docking was restrained to the active site area of the enzyme above the heme moiety and used default settings. Multiple simulations were performed for each substrate with consistent results for the preferred pose directionality and docking scores. Visualization of docked **C2**, **C5**, and **C8** in the active site was performed in Chimera.[22]

Time-Dependent Inhibition (TDI) Assays. Inhibition reactions contained 100 pmol purified rabbit CYP4B1, 200 pmol CPR, 100 pmol cytochrome b5, 10 μg of DLPC, 100 U catalase, and 50 μg of superoxide dismutase, in 50 mM KPi, pH 7.4, in a final volume of 125 μL. Compound **C5** or 1-aminobenzotriazole (ABT) was added from concentrated DMSO stocks to achieve a final concentration of 100 μM, and DMSO alone was also utilized as a vehicle control. DMSO concentration did not exceed 0.2%. Reactions were set up with and without 5 mM NAL and GSH to examine the effect of trapping agents on time-dependent inhibition. After 30 min on ice for reconstitution, the reactions were initiated by the addition of NADPH (1 mM final concentration). Aliquots of the inhibition reaction (25 μL) were taken at times ∼0 and 30 min, diluted 20-fold into a 0.5 mL probe substrate reaction containing lauric acid, at 10× the reported K_m for CYP4B1 (350 μM[23]), in 50 mM KPi buffer with 1 mM NADPH. The probe substrate reactions progressed for 10 min at 37 °C and were quenched

DOI: 10.1021/acs.chemrestox.9b00330
Chem. Res. Toxicol. XXXX, XXX, XXX−XXX

with 50 μL of 10% HCl. Subsequently, 10 nmol of 15-hydroxypentadecanoic acid was added as internal standard, and the solutions were extracted twice with 1 mL of ethyl acetate. The organic solvent was evaporated under a nitrogen stream, and the residues were redissolved in 50 μL of ethyl acetate. Then 50 μL of BSTFA reagent (Sigma) was added, and the silylation reactions were heated to 90 °C for 180 min. After cooling, the samples were analyzed by gas chromatography−mass spectrometry (GC−MS) on a Shimadzu QP2010 Gas Chromatograph Quadrupole mass spectrometer (Columbia, MD) with electron impact (EI) ionization using a previously reported method.[24]

RESULTS

CYP4B1-Mediated Cytotoxicity of *N*-Alkyl-3-furancarboxamide Analogs C1−C8. Previously, we demonstrated the utility of HepG2 cells stably transfected with CYP4B1 as a tool for investigating the potency of bioactivatable furan substrates that elicit cytotoxicity.[12,13] A series of *N*-alkyl-3-furancarboxamides (**C1−C8**, Figure 1A) were chosen to establish the optimal aliphatic chain-length for CYP4B1 furan substrate bioactivation. Dose-dependent toxicity was observed in CYP4B1-HepG2 cells with all eight compounds. A representative dose−response curve is shown for **C5** in Figure 1B. Compounds **C3**, **C4**, **C5**, and **C6** were the most potent cytotoxins exhibiting LD_{50} values 6 ± 1, 5 ± 1, 5 ± 1, and 5 ± 1 μM, respectively. CYP4B1-mediated cytotoxicity was greatly attenuated (one to two log-fold) when chain-length was shortened to < **C3** or lengthened beyond **C6**. LD_{50} values of 680 ± 40 and 24 ± 3 μM were measured for the short-chain compounds **C1** and **C2**, respectively, while LD_{50} values of 26 ± 3 and 130 ± 3 μM were measured for the long-chain compounds **C7** and **C8** (Figure 1A). No toxicity was observed in the control-HepG2 cells for any of the compounds, up to doses allowed by aqueous solubility.

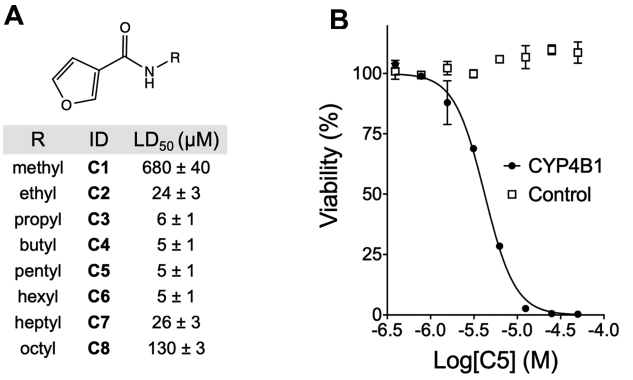

Figure 1. *N*-Alkylated 3-furancarboxamides (**C1−C8**) were synthesized to establish optimal aliphatic tail length for CYP4B1-mediated bioactivation, and compounds were utilized for cytotoxicity and metabolism assays. (A) LD_{50} values from CYP4B1-HepG2 cells dosed substrates **C1−C8**, and assayed for viability 72 h later, showed that **C3−C6** were the most potent congeners. Values presented are means ± SD from three to six replicates. (B) Representative dose−response curve for substrate **C5** illustrates the 5 μM LD_{50} detected in the CYP4B1-HepG2 cell line. No toxicity was observed in the control vector HepG2 cell line from exposure to **C5**, nor from any of the analogs up to doses outlined in the Experimental Procedures section.

Relative CYP4B1-Mediated Reactive Intermediate Formation from Compounds C1−C8. The nucleophile tandem of GSH and NAL was originally chosen for our studies due to (i) the stable pyrrole formation that occurs when a thiol and amine combination are added to oxidized furans[5,18,25] and (ii) the facile ability to track GSH-trapped reactive metabolites via neutral loss 129 scanning from different parent furan-containing compounds.[18] Preliminary work, performed with the same instrument settings as detailed in Experimental Procedures, showed that all eight parent compounds had ionization levels within ∼2-fold of each other. Presumably, the neutral loss of 129 is not greatly influenced by the species with which GSH reacts. Therefore, the combination of labile GSH fragmentation and similar parent ionization efficiency should enable semiquantitative comparisons between GSH/NAL-trapped adducts for the different compounds **C1−C8**. Although structurally more divergent homologues might be trapped with different efficiencies, we reasoned that the simple aliphatic modifications located away from the furan pharmacophore likely does not cause a serious quantitative complication.

Therefore, we could monitor CYP4B1-dependent bioactivation of compounds **C1−C8** by measuring the relative amounts of GSH/NAL-trapped pyrrole adduct generated from their respective reactive intermediates. **C1−C8-Adducts** were detected by neutral loss scanning and had base peak *m/z* values that matched a proposed pyrrole adduct structure with one each of GSH and NAL, and LC retention times that increased according to parent substrate chain length, as expected (Figure 2A,B). The relative amount of adduct formation was measured via PAR, with respect to the internal standard furafylline, and then normalized such that PAR was

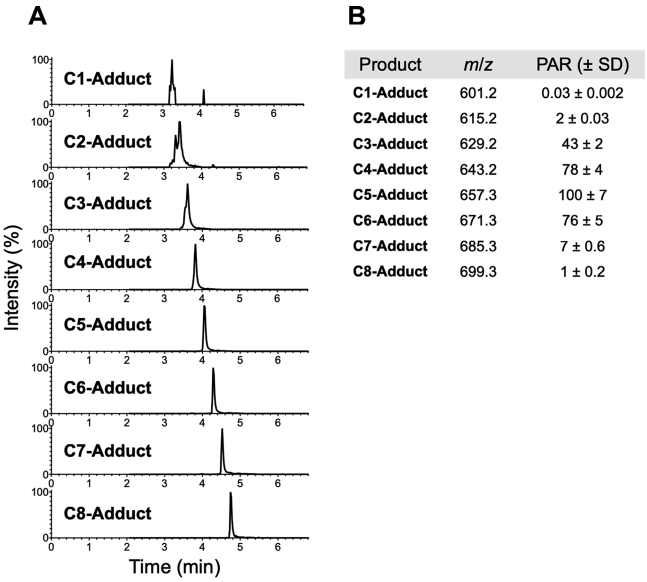

Figure 2. Assessment of GSH/NAL trapped reactive intermediates derived from substrates **C1−C8**. (A) Separate CYP4B1 incubations with **C1−C8**, in the presence of GSH (5 mM) and NAL (5 mM), each produced an NADPH-dependent metabolite adduct with a parent mass corresponding to a pyrrole structure containing one GSH and one NAL moiety (termed **C1−C8-Adduct**). Relative amounts of the adducts were evaluated via NL129 scanning and eluted according to parent chain length. Peak sizes have been normalized for viewing. Because of the short chromatographic separation, any different isomers present could not be resolved. (B) Average PAR values of the **C1−C8-Adduct** products with corresponding adduct *m/z*. Shown is the normalized average ± SD derived from three replicates. Compounds **C3−C6** produced substantially more trapped adduct than either the short (**C1**, **C2**) or long (**C7**, **C8**) chain homologues.

DOI: 10.1021/acs.chemrestox.9b00330
Chem. Res. Toxicol. XXXX, XXX, XXX−XXX

set to 100 for the **C5-Adduct**. The respective amounts generated from each substrate (average from three replicates ± SD) are shown in Figure 2B. Adduct PAR showed an elevated value for compounds **C3** through **C6** that inversely mirrored the LD_{50} values reported in Figure 1A. Short-chain compounds **C1** and **C2**, as well as long-chain compounds **C7** and **C8**, generated ∼10- to >100-fold less GSH/NAL-adduct than their midlength chain homologues.

MS/MS Characterization of CYP4B1-Mediated Formation of Isomeric C5-Adducts. For the simple comparative experiment above, we did not separate all isomeric products that were formed and could be detected with much longer chromatography runs. A detailed characterization was carried out on the pyrrole adducts formed from a fortified CYP4B1 incubation with compound **C5**. In the presence of GSH, NAL, and NADPH, CYP4B1 produced four isobaric metabolite peaks identified through an extended chromatographic separation followed by MS/MS analysis. These analytes eluted at retention times of 40.0, 40.8, 41.9, and 42.4 min and are numbered 1, 2, 3, and 4, respectively (Figure 3A). Each of these metabolites had an [M + H] peak at *m/z* 657.29 and likely represent different regio-isomers of a pyrrole adduct structure containing one NAL and one GSH moiety. Tandem MS of each analyte showed a fragment ion at *m/z* 528, indicative of a neutral loss of 129, as well as other diagnostic ions that are common fragments observed with GSH adducts (Figure 3B: isomer 1, Figure S2A,C: isomers 2 and 4). Isomer 3 lacked the characteristic GSH-adduct [M+H − 75] fragment ion that was present in each of the other three isomers at *m/z* 582. Therefore, 3 was suggested to be the result of a cyclization reaction, perhaps resulting from the free acid of the GSH-glycine moiety attacking a cyclic iminium intermediate. A possible structure, along with assigned fragmentation data, is shown in Figure S2B and D.

Characterization of Synthesized C5-GSH/NAL Adduct Standard. As a means of confirming our mass spectral evidence for the **C5-Adduct**, we synthesized a chemical standard of a **C5-GSH/NAL** adduct. Our synthesis produced a dominant species that matched the CYP4B1 incubation-derived **C5-Adduct** 1 by LC−MS at retention time 40.0 min (Figure 3A). The synthesized compound had an [M + H] peak at *m/z* 657.292 and exhibited the same MS/MS fragmentation pattern as observed for isomer 1 (Figure 3B,C). ^{1}H NMR analysis of the **C5-GSH/NAL** standard showed the presence of a pyrrole substructure and aliphatic protons consistent with side chain NAL and GSH moieties. Additional structural validation was performed via multiplicity-edited HSQC NMR (Figure S3). ROESY was used to characterize the GSH thiol attachment site to the pyrrole adduct from through-space proton interactions (Figure S4). The assignments specified the pyrrole protons as straddling the carboxamide with the GSH moiety attached adjacent to the NAL side chain. When tested with the aforementioned NL129 LC−MS/MS method, the synthesized **C5-GSH/NAL** adduct displayed a linear response from ∼1 nM to 10 μM. This broad range of linearity provided additional confidence in comparing relative adduct amounts deriving from compounds **C1**−**C8**. Of note, a very minor second peak that matched the retention time of adduct 2 was also present in the LC−MS chromatogram of the synthetic standard, but insufficient material was available for further NMR analysis.

Kinetics of CYP4B1-Mediated ω-Hydroxylation for C2, C5, and C8 and Adduct Formation for C5 of 3-Furancarboxamide Series. Preliminary experiments suggested that the major hydroxylation (+16) metabolite of the *N*-alkyl-3-furancarboxamides, produced by CYP4B1, occurred at the ω-position of the alkyl tail, although metabolism of both **C5** and **C8** produced additional mono-oxygenated products

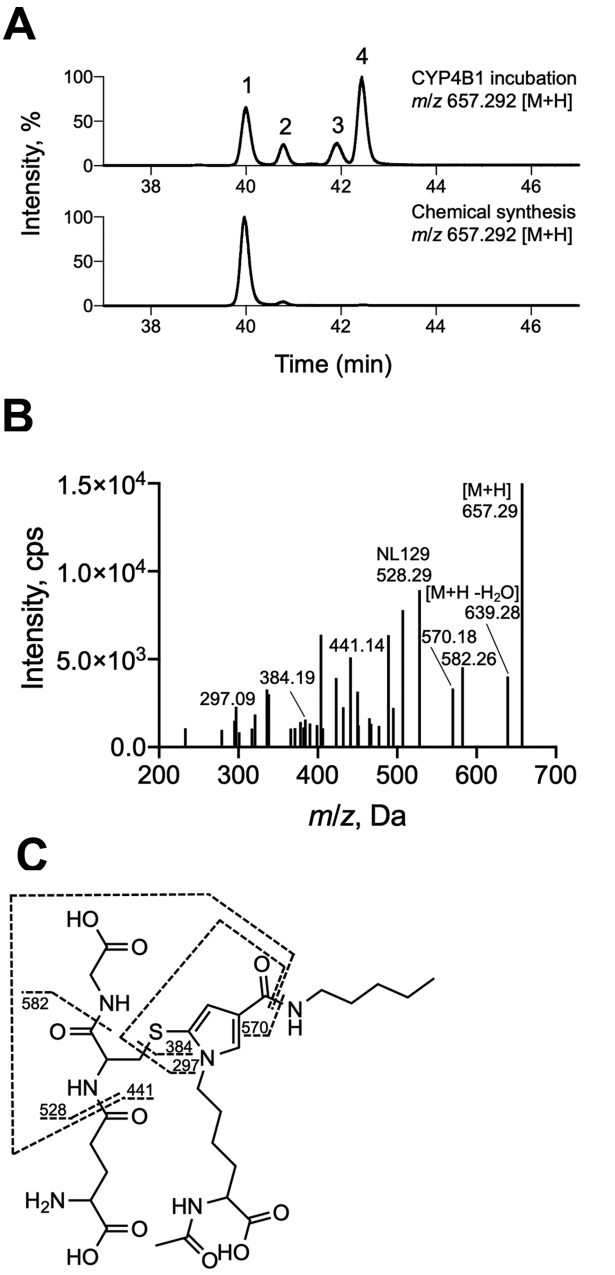

Figure 3. Characterization of GSH/NAL-containing **C5-Adducts**. (A) Extended chromatographic separation of the **C5-Adduct** from the CYP4B1 incubation revealed four isobaric species at *m/z* 657.292 (upper chromatogram). Chemical synthesis of a **C5-GSH/NAL** adduct produced one dominant species of the same mass, with the same chromatographic profile as isomer 1. A trace amount of isomer 2 at RT 40.8 min was also observed (lower chromatogram). (B) MS/MS analysis of isomer 1 was identical to that of the synthesized standard and produced ions typical of a GSH adduct. MS/MS spectra for isomers 2−4 is shown in the supplemental section. (C) Assigned structure for isomer 1, as elucidated from 2D-NMR techniques performed on the synthesized adduct (Figures S3 and S4), with annotated fragmentation pattern corresponding to the MS/MS spectrum.

DOI: 10.1021/acs.chemrestox.9b00330
Chem. Res. Toxicol. XXXX, XXX, XXX−XXX

that were tentatively assigned as the $\omega-1-$OH analogs (Figure S5). Therefore, compounds **C2**, **C5**, and **C8** were chosen (spanning the homologous series) as substrates for a kinetic analysis of CYP4B1-dependent ω-hydroxylation, following synthesis of the respective **C2**, **C5**, and **C8** ω-OH metabolites (Figure 4A–D). CYP4B1 exhibited kinetics consistent with the

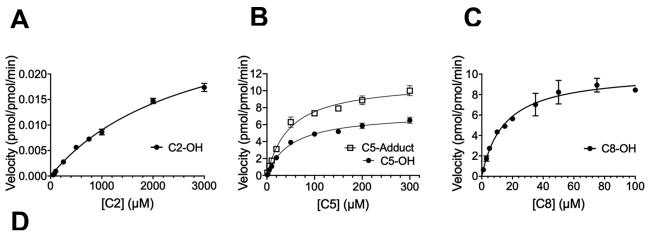

D

Biotransformation	K_m (μM)	V_{max} (min^{-1})	V_{max} / K_m (μM^{-1} min^{-1})
C2 → C2-OH	2740 ± 220	0.03 ± 0.003	1.2e-5
C5 → C5-OH	51.1 ± 4.8	7.4 ± 0.3	0.15
C5 → C5-Adduct	47.9 ± 3.4	11.1 ± 0.5	0.23
C8 → C8-OH	14.7 ± 0.3	10.2 ± 0.3	0.67

Figure 4. Kinetics for CYP4B1 metabolism of compounds **C2**, **C5**, and **C8**. (A) Rate assessment for ω-hydroxylation of **C2** (**C2-OH**), (B) **C5** (**C5-OH**), and (C) **C8** (**C8-OH**). (B) Kinetics for **C5** bioactivation and adduct (**C5-Adduct**) formation was also evaluated. (D) Kinetic constants for ω-hydroxylation showed a decrease in K_m and an overall increase in catalytic efficiency as the aliphatic chain was extended. The V_{max} for **C5-Adduct** formation was ~1.5-times that of **C5-OH**. Shown is the mean ± SD from three replicates.

Michaelis–Menten model for a single-substrate reaction for **C2**-, **C5**-, and **C8-ω-OH** formation, with K_m values of 2.7 mM, 51 μM, and 15 μM along with V_{max} values of 0.03, 7.4, and 10 pmol/pmol enzyme/min, respectively. Because of the fact that we were unable to achieve full apparent saturation with **C2**, the kinetic parameters calculated for this substrate should be treated as an approximation. The catalytic efficiencies for ω-hydroxylation of **C2**, **C5**, and **C8** by CYP4B1 increased substantially with increasing alkyl tail length, namely, 1.2e-5, 0.15, and 0.67 μM^{-1} min^{-1}, respectively.

With a characterized **C5-GSH/NAL** adduct standard (isomer 1) in hand, CYP4B1-mediated flux between reactive intermediate and ω-hydroxylation could be directly compared for compound **C5**. Metabolism of **C5** by CYP4B1 to the trapped **C5-Adduct** exhibited kinetics again consistent with the Michaelis–Menten model of a single-substrate reaction and apparent saturation by substrate was achieved. The K_m, V_{max}, and catalytic efficiency values for **C5** were calculated to be 48 μM, 11 pmol/pmol enzyme/min, and 0.23 μM^{-1} min^{-1}, respectively.

Investigation of Time-Dependent Inhibition of CYP4B1 by C5. A single concentration point, time-dependent inhibition assay was used to determine if the reactive electrophilic intermediates generated from compound **C5** (chosen due to the high amount of trapped reactive intermediate formation) were causing inactivation of CYP4B1. A 30 min inhibition preincubation (t_{30}) with compound **C5** showed a 44% reduction in CYP4B1 activity, as measured by the rate of lauric acid metabolism to the 11- and 12-OH metabolites (Figure 5). The 0 min preincubation (t_0) did not show any change relative to the vehicle control, indicating lack of both reversible and time-dependent inhibition after the dilution step for the probe substrate turnover. Incubation with the pan-CYP mechanism-based

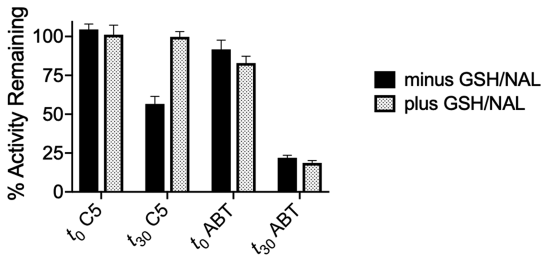

Figure 5. CYP4B1 time-dependent inhibition (TDI) investigation for compound **C5**. A 30 min (t_{30}) incubation of CYP4B1 with 100 μM **C5** and NADPH resulted in a ~44% reduction in enzyme activity, as normalized to vehicle control. Addition of GSH and NAL to the incubation abolished this observed TDI. The 0 min (t_0) incubation, prior to probe substrate turnover, shows **C5** is not engaging in reversible inhibition of CYP4B1. The pan-CYP inhibitor ABT was used as a positive control for MBI and was unaffected by the addition of the trapping agents GSH/NAL.

inhibitor 1-aminobenzotriazole[26] (ABT) resulted in 78% loss of activity for t_{30}, with minimal inactivation observed at t_0. Addition of the trapping agent combination, GSH and NAL, had no significant effect on t0 CYP4B1 activity; however, this condition completely abrogated the **C5** TDI for t_{30}. Upon bioactivation, a true mechanism-based inactivator reacts in the active site of the catalyzing enzyme and is not significantly affected by the addition of trapping agents. It is therefore possible that bioactivated **C5** causes its low amount of CYP4B1 TDI through reaction with nucleophilic surface amino acid residues belonging to CYP4B1 or CPR. TDI of CYP4B1 by ABT was not affected by the addition of GSH and NAL.

Docking of Compounds C2, C5, and C8 into the CYP4B1 Crystal Structure. The rabbit CYP4B1 crystal structure shows a narrow and hydrophobic active site, with residues Phe309, Leu485, Val375, and Val378 acting to confine aliphatic substrates, like *n*-octane.[20] The Gln218 and Tyr379 residues at the mouth of the boot-like binding pocket may participate in hydrogen-bonding to the carboxylate moiety of fatty acids or other electron-rich functionalities such as the furan in the 3-furancarboxamide series. As the carbon chain is lengthened for compounds **C2**, **C5**, and **C8**, docking studies predict increased affinity toward CYP4B1, generating scores that are approximations of ΔG values of −5.7, −6.7, and −7.4 kcal/mol, respectively. The top poses for **C2** and **C5** (Figure 6; colored yellow and green, respectively) position the furan ring above the heme for epoxidation, with the 4′ and 5′ carbons of the furan at 3.8 and 3.3 Å from the heme iron for both **C2** and **C5**. The top pose for **C8** (Figure 6; colored plum) reoriented the substrate with the aliphatic tail positioned over the heme for ω-hydroxylation, situating the terminal carbon 3.1 Å away from the heme iron. Additionally, the furan moiety oxygen of **C8** is located 3.3 and 3.6 Å from residues Gln218 and Tyr379, respectively. This is consistent with hydrogen-bonding contacts that may aid in terminal tail positioning for **C8**, which might explain the observed CYP4B1 preference for ω-hydroxylation of this substrate over epoxidation. The positions of these substrates in the CYP4B1 active site should not be considered as atomically exact, but as representative computational models consistent with our experimental data.

DOI: 10.1021/acs.chemrestox.9b00330
Chem. Res. Toxicol. XXXX, XXX, XXX–XXX

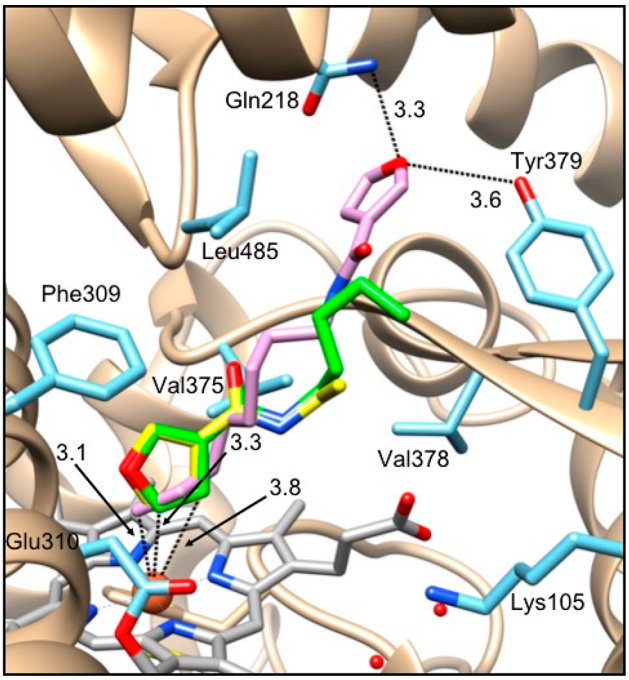

Figure 6. Docking of compounds **C2** (yellow), **C5** (green), and **C8** (plum) in the CYP4B1 crystal structure. The CYP4B1 active site contains hydrophobic residues Leu485, Val378, Val375, and Phe309 that aid in the enzyme's preference for aliphatic substrates. As the carbon tail chain length increases for **C2** through **C8**, improved affinity for these substrates is predicted. The preferred pose from multiple simulations showed both **C2** and **C5** positioned with their furan moiety located directly above the heme, with carbons at the 2′ and 3′ positions 3.3 and 3.8 Å away from the heme iron. The preferred pose for **C8** reversed this positioning, with the carbon tail now centered over the heme, 3.1 Å away from the iron. Gln218 and Tyr379 at the mouth of the active site may play a role in hydrogen-bond stabilization of the **C8** furan.

DISCUSSION

Of the known xenobiotics that undergo CYP4B1-mediated bioactivation, the natural products IPO and PK have been most extensively studied, both *in vitro* and *in vivo*, including the use of IPO in humans.[27] Given the potential liabilities of rapid glucuronidation and metabolism to inactivated products for IPO and PK, respectively, it seemed advantageous to investigate other structurally related compounds to identify new bioactivatable substrates for CYP4B1. The current study was begun with the principal goal of elucidating alkyl furan structure−activity relationships to better define elements of protoxicant potency and metabolism by the enzyme. Rabbit CYP4B1 is the most commonly studied form of the enzyme and its use as a suicide gene was first suggested in the 1990s.[33] In contrast to native human CYP4B1, rabbit CYP4B1 is both highly stable and efficiently bioactivates furan protoxicants to cytotoxic species. Although a re-engineered form of CYP4B1 with improved stability has been described recently,[4] we used rabbit CYP4B1 for all studies conducted here.

Substrates **C1**−**C8** were readily synthesized and proved to be an effective set of analogs to explore structure-metabolism relationships for CYP4B1. Upon testing in our assay, compounds **C3**−**C6** were the most potent cytotoxins in the CYP4B1-HepG2 cells, with LD_{50} values approximating that seen with IPO and PK of ∼5 μM.[12,13] From this we conclude that clearly (i) an alcohol (i.e., such as present in IPO) is not necessary for protoxicant effectiveness with CYP4B1, (ii) a 3′ positioned amide between the furan and tail substructure is an effective linker for preserving the chemical reactivity of furan metabolites, and (iii) an intermediary degree of aliphatic character is ideal for bioactivation. Additionally, compounds **C2**, **C5**, **C8** were shown to be stable to hydrolysis in complete tissue culture media because no significant decline in concentration was observed after 72 h (Figure S6). Consequently, conclusions drawn from studying this series is not confounded by undesirable hydrolytic reactions.

Because lipophilicity undoubtedly plays an important role in cellular permeability of the compounds, one might have surmised that **C8** would have been the most potent congener based on accumulated intracellular concentration. Therefore, the distinctive cytotoxicity profile we obtained prompted a biochemical analysis of the CYP4B1-dependent metabolism of **C1**−**C8** homologues. Congeneric pyrrole adducts derived from furan bioactivation were easily detected for **C1**−**C8** utilizing NL129 scanning. Upon investigating the relative amounts generated, normalized PAR for the adduct species were strikingly proportional to the cytotoxicity-dose response curve observed in whole HepG2 cells. The parabolic relationship seen between relative adduct amount and alkyl chain length strongly mirrored the relationship observed between cytotoxicity and alkyl chain length (Figure 7A), thereby demonstrating a tight relationship between furan bioactivation and cell death.

While clearly a useful tool in the analysis of xenobiotic metabolic liability, attempts to demonstrate a direct link between covalent binding and hepatotoxicity have been elusive. Historically, there are convincing examples showing the correlation between the covalent binding of reactive metabolites and liver necrosis.[28] However, as shown from metabolic analysis of hepato- and nonhepato-toxins, *in vitro* covalent binding studies, when analyzed alone, are not predictive of liver toxicity at least.[29] To our knowledge, the data presented here are unique in demonstrating a highly quantitative association between a covalent binding event (in this case the trapped reactive species formed) and cytotoxicity.

This strong correlation facilitates construction of a simple association model; a log−log plot of adduct PAR versus the LD_{50} results in a linear relationship (Figure 7B). If a power function does indeed model the dependency of cytotoxicity on reactive intermediate formation in this HepG2 system, then furan-containing congeners bioactivated by CYP4B1 that result in even higher quantities of electrophilic species would only show a nominal increase in potency. This is a unique finding that illustrates the robust association between these two variables that has not been observed to this degree before, and thus could have implications for future toxicological studies. A caveat is that the current research has not explored covalent binding of radiolabeled versions of these compounds, although we suggest a similar differential effect would be observed between amount of covalent binding generated *in vitro* and whole cell toxicity.

In general, trapping systems for reactive intermediates typically produce multiple adduct species.[25] Therefore, the **C5** furan was utilized for an in-depth interrogation of different conceivable pyrrole isomers that could be trapped from a CYP4B1 incubation. Previously, published research performed with the GSH/NAL system had either not investigated the possibility of multiple isomers formed or provided definitive structural assignments of the bioactivated and trapped furan-

DOI: 10.1021/acs.chemrestox.9b00330
Chem. Res. Toxicol. XXXX, XXX, XXX−XXX

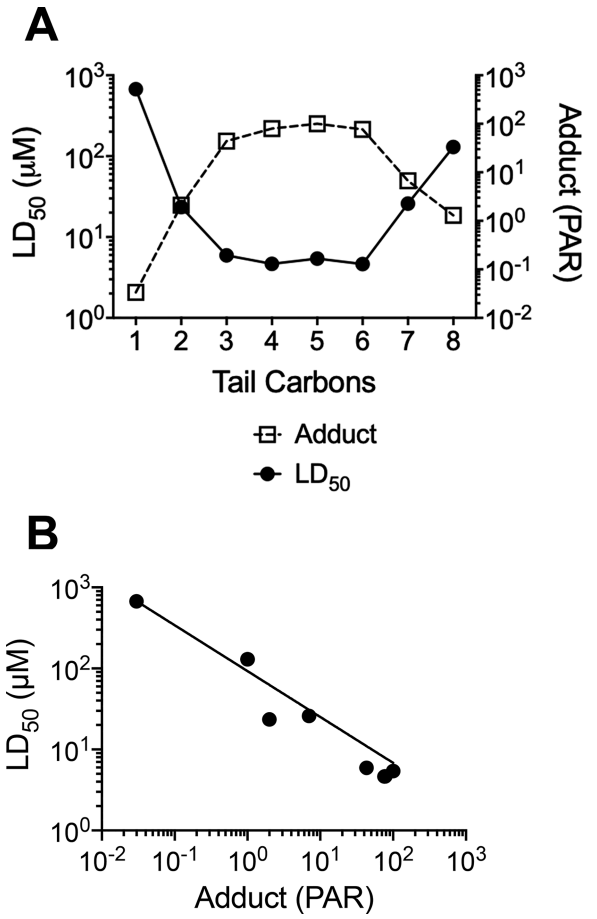

Figure 7. Correlation between CYP4B1-mediated reactive metabolite formation and cytotoxicity. (A) Parabolic relationship between the relative amount of **C1−C8-Adduct** formed from trapped reactive intermediate and alkyl chain length directly reflects the association between cytotoxic potency (as measured by LD_{50}) and alkyl chain length for **C1−C8**. Averages have been plotted, and standard deviations (reported earlier) have been omitted for clarity. (B) Linear dependency results from a log−log plot of normalized adduct amount versus LD_{50} and can be modeled by the equation $y = 2.6x^{-0.6} + 90.3x^{-0.6}$, which has been fit to the data; this is indicative of a power relationship between these two variables.

containing products.[18] Using an extended chromatography method with the GSH/NAL system, we detected two major and two minor isobaric **C5-Adducts** formed in an NADPH-dependent manner (Figure 3A, upper). MS/MS analysis for three of the isomers provided a rationale for the generation of the pyrrole adduct, while a fourth showed evidence for a cyclized variant, akin to that reported for GSH trapping of IPO.[30] The fragmentation data could not definitively assign the thiol attachment of GSH for these isomers. Therefore, we attempted to synthesize **C5-GSH/NAL** adduct standards to allow for their structural characterization. Interestingly, only one pyrrole adduct isomer could be isolated in abundance (potentially due to elevated temperature, differential stoichiometry of trapping agents, or solvents in the synthetic reaction compared to the biological incubation), which had the same LC−MS/MS profile as the metabolically generated isomer 1 (Figure 3A, lower). 2D NMR techniques enabled unambiguous determination of GSH attachment to the 5′ position of the pyrrole. We were thus able to assign a structure for the CYP4B1-generated isomer 1, which shows that **C5** is bioactivated and trapped by GSH/NAL in the same manner as IPO.[5] However, for **C5**, it is likely that both 1,2-addition and 1,4-addition by GSH, followed by NAL attack and condensation, contribute to the adducts formed (Figure 8). Note that all of these products are represented in the single peaks analyzed in a shorter chromatography run performed across all **C1−C8** analogs (Figure 2A). While other trapped species were also detected in CYP4B1 incubations with **C5** and GSH/NAL (a potential limitation with this nucleophile tandem), these were not explored in depth for this study.

Given the proclivity of CYP4B1 to ω-hydroxylate fatty acid substrates,[31] and the recent publication on PK metabolism by CYP4B1,[13] we hypothesized that as the aliphatic tail is lengthened for these compounds, substrate reorientation may occur in the active site of CYP4B1. This could result in a switching of metabolism from furan bioactivation to hydroxylation at the terminal end of the carbon chain, and thus lower the cytotoxic potency. A kinetic analysis of CYP4B1-dependent metabolism to the ω-hydroxyl metabolites of compounds **C2**, **C5**, and **C8** (chosen to span the series) indeed showed that catalytic efficiencies (V_{max}/K_m) for ω-hydroxylation increased substantially with tail length, peaking for **C8** at 0.67 μM^{-1} min^{-1} (Figure 4D).

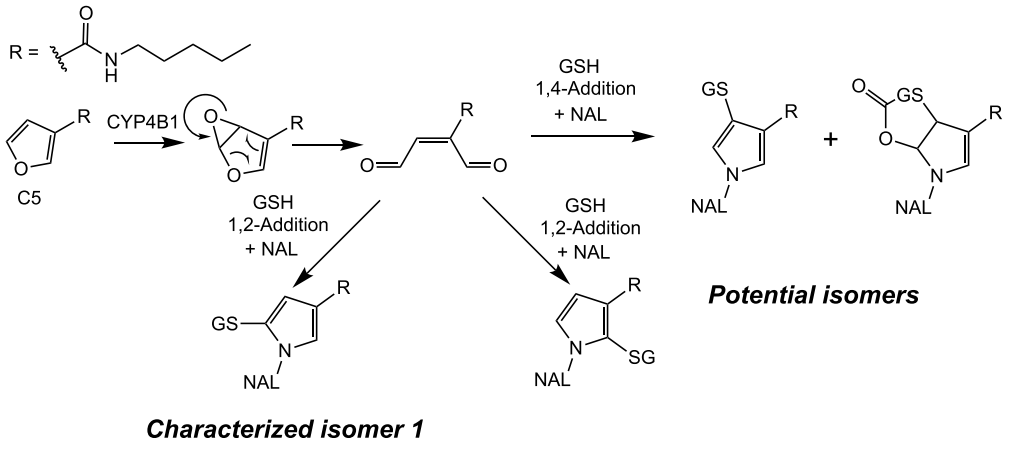

Figure 8. Proposed mechanism for the formation of GSH/NAL-trapped **C5-Adducts**. Characterized isomer 1 can be formed through 1,2-addition of GSH to the putative enedial species and reaction with NAL. Both 1,2- and 1,4-addition of GSH to the enedial and reaction with NAL may account for the additional **C5-Adducts** identified through LC−MS/MS; the structures for the potential isomers 2−4 are shown.

DOI: 10.1021/acs.chemrestox.9b00330
Chem. Res. Toxicol. XXXX, XXX, XXX−XXX

Additional kinetic studies were performed for **C5** metabolism by CYP4B1, to compare the relative rates of furan bioactivation versus ω-hydroxylation. Although most likely an underestimation of the total reactive metabolite amount generated, the V_{max} for the adduct was only 1.5-fold higher than that for the ω-hydroxylation process for **C5**. This is a key finding regarding future optimization of potency for CYP4B1 protoxicants since extensive (inactivating) hydroxylation may be a pharmacokinetic liability. Nonproductive metabolism to hydroxy metabolites could then render these compounds substrates for glucuronidation. We suggest further that potent protoxicants that undergo CYP4B1-mediated bioactivation with optimal tail length may benefit from fluorine substitution on the aliphatic moiety to block oxidation at terminal carbon positions.

To investigate differences in substrate binding to CYP4B1, compounds **C2**, **C5**, and **C8** were docked into the recently published CYP4B1 crystal structure.[20] The results indicated increased affinity as the carbon chain was lengthened, from a comparatively loosely bound **C2** to a much more tightly bound **C8**. Interestingly, the increased binding affinity for **C8** paralleled a preference for substrate reorientation, with the **C8** aliphatic tail, rather than its furan moiety, now oriented above the heme iron (Figure 6). This modeling matched extremely well to the trends we saw in the kinetic and metabolic data we acquired and bolsters the use of the CYP4B1 crystal structure for future substrate design work. Given our metabolic data and docking models that describe the interactions between CYP4B1 and *N*-alkyl-3-furancarboxamide analogs, the parabolic relationship between alkyl chain length and cytotoxicity may be rationalized by poorer binding of the shorter-chain compounds to CYP4B1 and increased oxidative metabolism for the longer chain compounds at sites distant from the furan warhead.

Numerous furan-containing compounds act as mechanism-based inactivators of CYPs.[25] The reactive intermediates that are generated in the CYP4B1-HepG2 system could partition between quenching by active site nucleophiles and escape from the CYP4B1 active site to cause cytotoxicity. To evaluate this potential flux, a TDI investigation was performed that showed a 44% loss of activity from **C5** treatment of CYP4B1 in the presence of NADPH. However, the addition of trapping agents completely nullified the small degree of enzyme inactivation observed ($k_{obs} \approx 0.02$ min^{-1} at 100 μM). This indicates that bioactivated **C5** is not a true mechanism-based inhibitor of CYP4B1 as assessed by the criteria given by Silverman.[32] In the absence of GSH and NAL, escaped reactive intermediate may cause some minimal time-dependent loss of enzyme activity through attachment to exterior amino acid residues on either CYP4B1 or CPR in this reconstituted system. We posit this would play a marginal role if the enzyme is expressed in target cells dosed with similar furan-containing congeners when excess biological nucleophiles, like GSH, are present in high concentration. Therefore, the CYP4B1 active site architecture likely insulates the enzyme from self-inactivation and contributes to its efficient cytotoxic action.

In summary, we have undertaken an in-depth characterization of the structural elements required for potent IPO-like congeners that undergo CYP4B1 bioactivation to elicit whole cell toxicity. *N*-Alkyl-3-furancarboxamides are stable, easily synthesized for analog and library generation, and possess a similar cytotoxicity and reactivity profile as their ketone counterparts. When these congeners are affixed with 3−6 tail carbons, they are highly toxic in HepG2 cells expressing CYP4B1 and elicit no observed effect in control vector cells. Reducing aliphatic character lowers the affinity of these substrates for the enzyme, while extending the tail increases ω-hydroxylation rates; both of which lower the potency for CYP4B1-mediated cytotoxicity. Relative amounts of trapped reactive intermediates formed from CYP4B1 metabolism of these substrates with GSH and NAL are strikingly correlated to cytotoxicity; to our knowledge, a comparison like this has never been shown to this high degree. This effect may be explained due in large part to the efficient nature by which the reactive intermediates are able to escape the CYP4B1 active site without causing measurable mechanism-based inactivation. These studies further demonstrate the utility of CYP4B1 for use in suicide gene systems, especially in settings requiring highly controlled cytotoxicity. Future studies will investigate the utility of fluorinated congeners and probe the specificity of bioactivation by hepatic CYPs, particularly CYP1A2.

■ ASSOCIATED CONTENT

Supporting Information

The Supporting Information is available free of charge at https://pubs.acs.org/doi/10.1021/acs.chemrestox.9b00330.

Western blot assessment of CYP4B1 expression levels in HepG2 cells; MS/MS fragmentation data for **C5-Adduct** isomers 2−4; HSQC structural validation for **C5-GSH/NAL**; ROESY characterization of **C5-GSH/NAL**; **C2-**, **C5-**, **C8-OH** metabolite identification; *N*-alkyl-3-furancarboxamide stability assessment in tissue culture media; NMR spectroscopy; annotated ^{1}H NMR: **C1−C8** and **C2-OH**, **C5-OH**, **C8-OH** (PDF)

■ AUTHOR INFORMATION

Corresponding Author

*E-mail: Rettie@uw.edu.

ORCID

John P. Kowalski: 0000-0002-0343-8425

Miklos Guttman: 0000-0003-2419-1334

Funding

Brady Fund for Natural Products, NIH T32 Pharmacological Sciences Training Grant, Strategic Research Fund of the Heinrich-Heine University, Düsseldorf, Germany.

Notes

The authors declare no competing financial interest.

■ ACKNOWLEDGMENTS

We would like to thank Dr. Tim Martins (Quellos, Seattle) for assistance with preliminary screening efforts.

■ ABBREVIATIONS

CYP4B1, cytochrome P450 4B1; IPO, 4-ipomeanol; PK, perilla ketone; UGT, uridine 5'-diphosphoglucuronosyl transferase; CPR, cytochrome P450 reductase; NAL, *N*-α-acetyl-L-lysine; KPi, potassium phosphate buffer; NL129, neutral loss scanning of 129 Da; MRM, multiple reaction monitoring; PAR, peak area ratio; TDI, time-dependent inhibition; ABT, 1-aminobenzotriazole; **C1−C8**, *N*-alkyl-3-furancarboxamide compounds with aliphatic tails of one through eight carbons; **C5-Adduct**, GSH/NAL trapped adduct(s) from CYP4B1 bioactivation of **C5**

DOI: 10.1021/acs.chemrestox.9b00330
Chem. Res. Toxicol. XXXX, XXX, XXX−XXX

REFERENCES

(1) Edson, K. Z., and Rettie, A. E. (2013) CYP4 enzymes as potential drug targets: focus on enzyme multiplicity, inducers and inhibitors, and therapeutic modulation of 20-hydroxyeicosatetraenoic acid (20-HETE) synthase and fatty acid omega-hydroxylase activities. *Curr. Top. Med. Chem. 13*, 1429−1440.

(2) Baer, B. R., and Rettie, A. E. (2006) CYP4B1: an enigmatic P450 at the interface between xenobiotic and endobiotic metabolism. *Drug Metab. Rev. 38*, 451−476.

(3) Zheng, Y. M., Fisher, M. B., Yokotani, N., Fujii-Kuriyama, Y., and Rettie, A. E. (1998) Identification of a meander region proline residue critical for heme binding to cytochrome P450: implications for the catalytic function of human CYP4B1. *Biochemistry 37*, 12847−12851.

(4) Wiek, C., Schmidt, E. M., Roellecke, K., Freund, M., Nakano, M., Kelly, E. J., Kaisers, W., Yarov-Yarovoy, V., Kramm, C. M., Rettie, A. E., and Hanenberg, H. (2015) Identification of amino acid determinants in CYP4B1 for optimal catalytic processing of 4-ipomeanol. *Biochem. J. 465*, 103−114.

(5) Baer, B. R., Rettie, A. E., and Henne, K. R. (2005) Bioactivation of 4-ipomeanol by CYP4B1: adduct characterization and evidence for an enedial intermediate. *Chem. Res. Toxicol. 18*, 855−864.

(6) Roellecke, K., Virts, E. L., Einholz, R., Edson, K. Z., Altvater, B., Rossig, C., von Laer, D., Scheckenbach, K., Wagenmann, M., Reinhardt, D., Kramm, C. M., Rettie, A. E., Wiek, C., and Hanenberg, H. (2016) Optimized human CYP4B1 in combination with the alkylator prodrug 4-ipomeanol serves as a novel suicide gene system for adoptive T-cell therapies. *Gene Ther. 23*, 615−626.

(7) Bonini, C., and Mondino, A. (2015) Adoptive T-cell therapy for cancer: The era of engineered T cells. *Eur. J. Immunol. 45*, 2457−2469.

(8) Ciceri, F., Bonini, C., Gallo-Stampino, C., and Bordignon, C. (2005) Modulation of GvHD by suicide-gene transduced donor T lymphocytes: clinical applications in mismatched transplantation. *Cytotherapy 7*, 144−149.

(9) Turtle, C. J., Hanafi, L. A., Berger, C., Gooley, T. A., Cherian, S., Hudecek, M., Sommermeyer, D., Melville, K., Pender, B., Budiarto, T. M., Robinson, E., Steevens, N. N., Chaney, C., Soma, L., Chen, X., Yeung, C., Wood, B., Li, D., Cao, J., Heimfeld, S., Jensen, M. C., Riddell, S. R., and Maloney, D. G. (2016) CD19 CAR-T cells of defined CD4+:CD8+ composition in adult B cell ALL patients. *J. Clin. Invest. 126*, 2123.

(10) Statham, C. N., Dutcher, J. S., Kim, S. H., and Boyd, M. R. (1982) Ipomeanol 4-glucuronide, a major urinary metabolite of 4-ipomeanol in the rat. *Drug Metab. Dispos. 10*, 264−267.

(11) Parkinson, O. T., Teitelbaum, A. M., Whittington, D., Kelly, E. J., and Rettie, A. E. (2016) Species Differences in Microsomal Oxidation and Glucuronidation of 4-Ipomeanol: Relationship to Target Organ Toxicity. *Drug Metab. Dispos. 44*, 1598−1602.

(12) Teitelbaum, A. M., McDonald, M. G., Kowalski, J. P., Parkinson, O. T., Scian, M., Whittington, D., Roellecke, K., Hanenberg, H., Wiek, C., and Rettie, A. E. (2019) Influence of Stereochemistry on the Bioactivation and Glucuronidation of 4-Ipomeanol. *J. Pharmacol. Exp. Ther. 368*, 308−316.

(13) Roellecke, K., Jager, V. D., Gyurov, V. H., Kowalski, J. P., Mielke, S., Rettie, A. E., Hanenberg, H., Wiek, C., and Girhard, M. (2017) Ligand characterization of CYP4B1 isoforms modified for high-level expression in Escherichia coli and HepG2 cells. *Protein Eng., Des. Sel. 30*, 205−216.

(14) Cheesman, M. J., Baer, B. R., Zheng, Y. M., Gillam, E. M., and Rettie, A. E. (2003) Rabbit CYP4B1 engineered for high-level expression in Escherichia coli: ligand stabilization and processing of the N-terminus and heme prosthetic group. *Arch. Biochem. Biophys. 416*, 17−24.

(15) Chen, W., Koenigs, L. L., Thompson, S. J., Peter, R. M., Rettie, A. E., Trager, W. F., and Nelson, S. D. (1998) Oxidation of acetaminophen to its toxic quinone imine and nontoxic catechol metabolites by baculovirus-expressed and purified human cytochromes P450 2E1 and 2A6. *Chem. Res. Toxicol. 11*, 295−301.

(16) Schmidt, E. M., Wiek, C., Parkinson, O. T., Roellecke, K., Freund, M., Gombert, M., Lottmann, N., Steward, C. A., Kramm, C. M., Yarov-Yarovoy, V., Rettie, A. E., and Hanenberg, H. (2015) Characterization of an Additional Splice Acceptor Site Introduced into CYP4B1 in Hominoidae during Evolution. *PLoS One 10*, No. e0137110.

(17) Hyster, T. K., and Rovis, T. (2010) Rhodium-catalyzed oxidative cycloaddition of benzamides and alkynes via C-H/N-H activation. *J. Am. Chem. Soc. 132*, 10565−10569.

(18) Li, C., Lin, D., Gao, H., Hua, H., Peng, Y., and Zheng, J. (2015) N-Acetyl Lysine/Glutathione-Derived Pyrroles as Potential Ex Vivo Biomarkers of Bioactivated Furan-Containing Compounds. *Chem. Res. Toxicol. 28*, 384−393.

(19) Trott, O., and Olson, A. J. (2009) Auto Dock Vina: improving the speed and accuracy of docking with a new scoring function, efficient optimization and multithreading. *J. Comput. Chem. 31*, 455−461.

(20) Hsu, M. H., Baer, B. R., Rettie, A. E., and Johnson, E. F. (2017) The Crystal Structure of Cytochrome P450 4B1 (CYP4B1) Monooxygenase Complexed with Octane Discloses Several Structural Adaptations for omega-Hydroxylation. *J. Biol. Chem. 292*, 5610−5621.

(21) O'Boyle, N. M., Banck, M., James, C. A., Morley, C., Vandermeersch, T., and Hutchison, G. R. (2011) Open Babel: An open chemical toolbox. *J. Cheminf. 3*, 33.

(22) Pettersen, E. F., Goddard, T. D., Huang, C. C., Couch, G. S., Greenblatt, D. M., Meng, E. C., and Ferrin, T. E. (2004) UCSF Chimera–a visualization system for exploratory research and analysis. *J. Comput. Chem. 25*, 1605−1612.

(23) Baer, B. R., Schuman, J. T., Campbell, A. P., Cheesman, M. J., Nakano, M., Moguilevsky, N., Kunze, K. L., and Rettie, A. E. (2005) Sites of covalent attachment of CYP4 enzymes to heme: evidence for microheterogeneity of P450 heme orientation. *Biochemistry 44*, 13914−13920.

(24) McDonald, M. G., Ray, S., Amorosi, C. J., Sitko, K. A., Kowalski, J. P., Paco, L., Nath, A., Gallis, B., Totah, R. A., Dunham, M. J., Fowler, D. M., and Rettie, A. E. (2017) Expression and Functional Characterization of Breast Cancer-Associated Cytochrome P450 4Z1 in Saccharomyces cerevisiae. *Drug Metab. Dispos. 45*, 1364−1371.

(25) Peterson, L. A. (2013) Reactive metabolites in the biotransformation of molecules containing a furan ring. *Chem. Res. Toxicol. 26*, 6−25.

(26) de Montellano, P. R. O. (2018) 1-Aminobenzotriazole: A Mechanism-Based Cytochrome P450 Inhibitor and Probe of Cytochrome P450 Biology. *Med. Chem. (Los Angeles, CA, U. S.) 8*, 38.

(27) Rowinsky, E. K., Noe, D. A., Ettinger, D. S., Christian, M. C., Lubejko, B. G., Fishman, E. K., Sartorius, S. E., Boyd, M. R., and Donehower, R. C. (1993) Phase I and pharmacological study of the pulmonary cytotoxin 4-ipomeanol on a single dose schedule in lung cancer patients: hepatotoxicity is dose limiting in humans. *Cancer Res. 53*, 1794−1801.

(28) Gillette, J. R. (1974) Commentary. A perspective on the role of chemically reactive metabolites of foreign compounds in toxicity. I. Correlation of changes in covalent binding of reactivity metabolites with changes in the incidence and severity of toxicity. *Biochem. Pharmacol. 23*, 2785−2794.

(29) Obach, R. S., Kalgutkar, A. S., Soglia, J. R., and Zhao, S. X. (2008) Can in vitro metabolism-dependent covalent binding data in liver microsomes distinguish hepatotoxic from nonhepatotoxic drugs? An analysis of 18 drugs with consideration of intrinsic clearance and daily dose. *Chem. Res. Toxicol. 21*, 1814−1822.

(30) Chen, L. J., DeRose, E. F., and Burka, L. T. (2006) Metabolism of furans in vitro: ipomeanine and 4-ipomeanol. *Chem. Res. Toxicol. 19*, 1320−1329.

(31) Fisher, M. B., Zheng, Y. M., and Rettie, A. E. (1998) Positional specificity of rabbit CYP4B1 for omega-hydroxylation1 of short-medium chain fatty acids and hydrocarbons. *Biochem. Biophys. Res. Commun. 248*, 352−355.

(32) Silverman, R. B. (1988) *Mechanism-Based Enzyme Inactivation: Chemistry and Enzymology*; CRC Press.

DOI: 10.1021/acs.chemrestox.9b00330
Chem. Res. Toxicol. XXXX, XXX, XXX−XXX

(33) Rainov, N. G., Sena-Esteves, M., Fraefel, C., Dobberstein, K. U., Chiocca, E. A., and Breakefield, X. O. (1998) A chimeric fusion protein of cytochrome CYP4B1 and green fluorescent protein for detection of pro-drug activating gene delivery and for gene therapy in malignant glioma. *Advances in experimental medicine and biology 451*, 393.

DOI: 10.1021/acs.chemrestox.9b00330
Chem. Res. Toxicol. XXXX, XXX, XXX−XXX